JOURNAL OF AIRCRAFT
Vol. 47, No. 4, July–August 2010

Effective Approach to Characterization of Prediction Errors for Balloon Ascent Trajectories

Roberto Palumbo,* Gianfranco Morani,† and Federico Corraro‡
Centro Italiano Ricerche Aerospaziali, 81043 Capua, Italy

DOI: 10.2514/1.47005

To comply with the objectives of a balloon flight, it is usually necessary to predict, monitor and track the trajectory. Within the framework of the Unmanned Space Vehicles program, the Italian Aerospace Research Center developed several methodologies useful to evaluate balloon mission feasibility, predict balloon trajectory, and assess trajectory prediction errors. These methodologies are based on weather forecast data obtained using the Integrated Forecast System model by the European Center for Medium-Range Weather Forecast and on the use of a proprietary simulation software for the prediction of flight trajectory and thermal behavior of zero-pressure balloons. In this paper, we propose an effective approach for the characterization of trajectory prediction error based on statistical characterization of the forecast error of the Integrated Forecast System atmospheric data (winds, temperature, and pressure), statistical characterization of the error on gas mass due to inflation procedures, and analytical error propagation of these sources of uncertainties on the balloon's velocity vector. The proposed approach allows estimating the actual trajectory dispersion once the predicted trajectory is computed using forecast data. The methodology proposed improves the trajectory prediction methodology that was successfully used during the first Dropped Transonic Flight Test accomplished by Italian Aerospace Research Center.

Nomenclature

A_D	=	reference area for drag force computation, m^2
A_{eff}	=	reference area for convective heat load computation, m^2
C_D	=	drag force coefficient
c_v	=	specific heat at constant volume of the lifting gas (for Helium: 3121.5 J/kg/K)
e_ϑ	=	longitude prediction error, deg
e_λ	=	latitude prediction error, deg
g	=	gravity acceleration, m/s^2
h	=	altitude, m
h_{conv}	=	internal convection heat transfer coefficient, $W/m^2/K$
M_{gas}	=	mass of gas, kg
M_{gross}	=	total load mass, kg
$P(s)$	=	first-order low-pass filter
Q_{IntConv}	=	internal convective heat load, W
R_{air}	=	specific gas constant of air (287.05 J/kg/K)
R_e	=	projection of Earth radius on local parallel, m
R_{gas}	=	specific gas constant of the lifting gas (for helium: 2078.5 J/kg/K)
R_n	=	Earth radius, m
R_x	=	autocorrelation function of the stochastic process x
$R_{\Delta M_{\text{gas}}}$	=	autocorrelation function of the gas mass error, kg^2
$R_{\Delta p_{\text{air}}}$	=	autocorrelation function of the air pressure forecast error, Pa^2
$R_{\Delta T_{\text{air}}}$	=	autocorrelation function of the air temperature forecast error, K^2
$R_{\Delta V_E}$	=	autocorrelation function of the wind forecast error (east component), m^2/s^2
$R_{\Delta V_N}$	=	autocorrelation function of the wind forecast error (north component), m^2/s^2
T_{film}	=	balloon film bulk temperature, K
T_{gas}	=	gas (helium) Temperature, K
t_h	=	instant at which the predicted ascent trajectory reaches altitude h, s
vol	=	balloon volume, m^3
V_E	=	east velocity component, m/s
V_N	=	north velocity component, m/s
V_z	=	rate of climb of the balloon, m/s
w	=	Gaussian white noise
γ	=	specific heats ratio, c_p/c_v
ϑ	=	longitude, deg
λ	=	latitude, deg
ρ_{air}	=	atmospheric density, kg/m^3
ρ_{gas}	=	gas (helium) density, kg/m^3
σ	=	ratio between the molecular weight of the air and the molecular weight of the gas
σ_{e_ϑ}	=	standard deviation of longitude prediction error, deg
σ_{e_λ}	=	standard deviation of latitude prediction error, deg
σ_w^2	=	variance of the Gaussian white noise w
τ	=	time constant of the first-order low-pass filter $P(s)$

Subscripts

fc	=	forecast quantity
nom	=	nominal quantity

Presented as Paper 2009-2803 at the AIAA Balloon Systems Conference, Seattle, WA, 4–7 May 2009; received 25 September 2009; revision received 18 January 2010; accepted for publication 1 February 2010. Copyright © 2010 by the American Institute of Aeronautics and Astronautics, Inc. All rights reserved. Copies of this paper may be made for personal or internal use, on condition that the copier pay the $10.00 per-copy fee to the Copyright Clearance Center, Inc., 222 Rosewood Drive, Danvers, MA 01923; include the code 0021-8669/10 and $10.00 in correspondence with the CCC.

*Researcher, Guidance Navigation and Control Laboratory, Via Maiorise; r.palumbo@cira.it. Senior Member AIAA.

†Researcher, Guidance Navigation and Control Laboratory, Via Maiorise; g.morani@cira.it.

‡Head, Guidance Navigation and Control Laboratory, Via Maiorise; f.corraro@cira.it.

I. Introduction

SCIENTIFIC balloons allow a unique and cost-effective way to carry out many experiments in a near-space environment. Generally, balloons are used as observation platforms for atmospheric studies or as carrier systems of particular instruments for research purposes or even as drop towers for flight tests of specific payloads. In any case, balloon mission planning is a challenging problem. Mission objectives and safety constraints often require specific flight trajectories; therefore, trajectory prediction is an important, yet difficult, matter. Indeed, after liftoff, a balloon can be considered as a thermal and dynamical system that is practically in free evolution inside a complex thermal environment and subject to

atmospheric winds. Consequently, balloon mission preparation requires an accurate and reliable trajectory prediction methodology in order to accomplish the mission successfully.

In recent years, the Italian Aerospace Research Center (CIRA) has acquired valuable experience in the field of scientific ballooning. Within the framework of CIRA's program named Unmanned Space Vehicles (USV), CIRA has developed several methodologies and tools in the fields of meteorological conditions forecast and balloon trajectory prediction and optimization [1]. The objective of the USV project is to design and manufacture two unmanned vehicles (FTB1 for atmospheric flights and FTBX for sustained hypersonic flight), conceived as flying laboratories, in order to test and verify advanced functionalities and critical operational aspects peculiar of the future reusable launch vehicles [2]. The nominal atmospheric mission profile (named Dropped Transonic Flight Test, DTFT) is based on a drop of the FTB1 vehicle from a stratospheric balloon at high altitudes, between 20 and 30 km, inside a specific target area located in the Tyrrhenian Sea, lifting off from a launch base located in Arbatax, Sardinia, Italy (see Fig. 1). Therefore, weather forecast considerations and balloon trajectory prediction are vital for mission operations and mission success. The first DTFT mission (DTFT1) was carried out on 24 Feb. 2007. Currently, CIRA is working on the next flight test, the DTFT2 mission, which will take place during the next years.

In the last years, some efforts have been made to develop accurate trajectory prediction for stratospheric balloons ([3–5] and references therein). In these papers, balloon trajectory prediction is performed taking into account several trajectory prediction sources of uncertainty (wind velocity, gas mass, air temperature, etc.). In particular, wind uncertainty is computed using forecast models as well as soundings. This is accomplished through a statistical analysis on the distance between the predicted and actual trajectories. The analysis results are then used to compute the levels of probability related to the interception of a target area for each predicted trajectory. The obtained results, however, could be heavily dependent on the altitude profile chosen for the analysis, with the distance between the trajectories being strongly related to the time to reach the target point.

In a previous work by the present authors [6], a methodology for the prediction and optimization of the ascent trajectory of a stratospheric balloon was developed, based on the characterization of the wind forecast error. The authors showed that this characterization is almost independent of the actual balloon ascent rate, making this approach more general and effective regardless of the altitude profile. This methodology was successfully applied to the preparation and the planning of the DTFT1 mission.

Although effective, the previous approach had several limitations: first, the uncertainty on the vertical velocity component of the balloon was neglected. This source of uncertainty is mostly related to the atmospheric forecast data (air temperature and pressure), to the gas mass, and to the thermodynamic model used to simulate the balloon ascent. In [6] the influence of the errors on air temperature and pressure was not evaluated and the uncertainty on the gas mass due to inflation procedures was not explicitly taken into account in the computation of the dispersion areas of the balloon ascent trajectory. Moreover, the characterization of the wind forecast error was carried out comparing a large set of simulated balloon trajectories obtained using the available wind forecast and analysis data, thus requiring a huge computational effort. In addition, the estimation of the trajectory prediction error was carried out numerically starting from the aforementioned characterization.

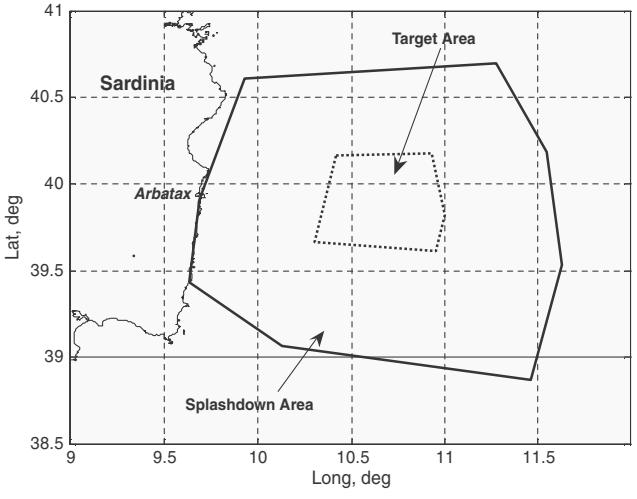

Fig. 1 Target area/safe splashdown area.

In this paper, we describe a more general approach to the propagation of the uncertainties on the balloon's velocity vector. We present a methodology that allows taking into account a broader set of uncertain variables, including the air temperature, air pressure, and gas mass. Moreover, the characterization of the forecast error is performed using the atmospheric data only (without relying on simulated trajectories), and the trajectory prediction error is computed analytically starting from this characterization. This allows reducing the computational effort and, at the same time, it allows guaranteeing a more reliable dispersion along the predicted ascent trajectory. The development of the methodology is demonstrated using ACHAB (Analysis Code for High-Altitude Balloons), a proprietary simulation tool for the prediction of flight trajectory and thermal behavior of high-altitude zero-pressure balloons (see [7]).

As in [6], errors due to the balloon thermodynamic model will not be considered in this paper. They are discussed in [7] and, in any case, their effect on the ascent trajectory cannot be reliably evaluated due to the lack of a significant set of real ascent trajectories.

The paper is organized as follows. An overview of the main uncertain variables that affect the balloon ascent trajectory is given in Sec. II. The description of the methodological approach is given in Sec. III. Results are reported in Sec. IV. Finally, Sec. V contains some brief concluding remarks.

II. Sources of Uncertainty

The ascent portion of the trajectory of a balloon is affected by several sources of uncertainty. In the following, a brief description of these sources of uncertainty will be given.

A. Wind Forecast

Horizontal motion of a balloon is mainly driven by atmospheric winds. Actually, the assumption that the horizontal velocity of the balloon is considered to be always equal to the horizontal velocity of the wind is quite accurate. Strictly speaking, this assumption implies instant adjustment of the horizontal velocity as the balloon moves from one air stratum to another in which the wind velocity is different (see [8]). It should be noted that such behavior does not reflect what actually happens during some of the flight phases (liftoff, tropopause transition, stratospheric oscillations, or local wind shears). Nevertheless, it can be globally considered to be true, because the average acceleration over long portions of the flight is always practically zero. Therefore, an accurate prediction of the wind velocities is essential for an accurate trajectory prediction; consequently, uncertainties on the wind forecast are directly propagated on the horizontal velocity vector of the balloon.

Our trajectory predictions are performed using ACHAB [7] and considering the wind forecast data coming from the Integrated Forecast System (IFS), a deterministic global model by the European Center for Medium-Range Weather Forecast (ECMWF). Uncertainties on these forecasts have to be taken into account to evaluate the trajectory dispersion accurately.

B. Mass of Gas Transferred to the Balloon at Inflation

Balloons are usually inflated with a predetermined amount of gas mass M_{gas} in order to ensure that the balloon will have a certain nominal free lift. Unfortunately, there is uncertainty in the quantity of gas transferred to the balloon at liftoff. In fact, the inflation procedures that are commonly followed to allow the transfer of the

desired amount of gas to the balloon heavily rely on the measurement of static pressure and temperature of the gas while the gas itself is being withdrawn from the tanks [8]. However, neither gas pressure nor temperature can be measured accurately during this operation. Moreover, the procedure is based on the use of an approximate thermodynamic transformation that relates the initial (equilibrium) static pressure and temperature to the final (measured) pressure. This final cutoff pressure ensures that the desired amount of lift has been transferred to the balloon. Consequently, this procedure is affected by several measurement errors and model approximations. Experience shows that the uncertainty on the gas mass due to inflation procedures is in the range of 1 to 2% [9].

C. Air Temperature and Air Pressure Forecast

Air pressure p_{air} and air temperature T_{air} are variables that directly influence the buoyancy force. Therefore, the uncertainty on these quantities is directly propagated to the vertical velocity. As for the wind data, air pressure and air temperature forecast data come from the ECMWF model. Uncertainties on these forecasts have to be taken into account to evaluate the trajectory dispersion.

D. Thermodynamic Model Uncertainties

A balloon is a thermal system that moves inside a complex thermal environment. Trajectory prediction is carried out using a simulation model (ACHAB) that is able to simulate the thermal behavior of zero-pressure balloons. Consequently, modeling errors may influence the trajectory prediction and should be taken into account. In this paper, we will not discuss the effects of these sources of uncertainties. They are briefly discussed in [7] and, in any case, their effect on the ascent trajectory cannot be reliably evaluated due to the lack of a significant set of real ascent trajectories. However, common ballooning practice suggests that modeling errors may be often regarded as less influential than those related to the other sources of uncertainty (such as wind and gas mass uncertainties) [4].

III. Characterization of the Trajectory Prediction Error

To characterize the trajectory prediction error, it is necessary to propagate the aforementioned uncertainties on the balloon's velocity vector. To develop the mathematical approach, it is convenient to define certain variables. Let us define the east and north components of the wind velocity that, as stated in Sec. II, are assumed to be equal to the east and north velocity components of the balloon:

$$V_E(t) \stackrel{\text{def}}{=} R_e \dot{\vartheta}(t) \frac{\pi}{180} \qquad V_N(t) \stackrel{\text{def}}{=} R_n \dot{\lambda}(t) \frac{\pi}{180} \tag{1}$$

where $\dot{\vartheta}$ and $\dot{\lambda}$ are the rate of change of longitude and the latitude with respect to time (in degrees per second), and R_n and R_e are the Earth's radius and its projection on the local parallel, respectively.

We will describe here the mathematical approach, considering only the east velocity component (the same conclusions obviously hold for the north component).

Integrating Eq. (1) with respect to time, we have

$$\vartheta(t_h) = \frac{180}{\pi R_e} \int_0^{t_h} V_E(t)\, \mathrm{d}t \tag{2}$$

where t_h is the time instant at which the trajectory reaches the altitude h.

Performing a change of variables (from the variable time to the variable altitude), we obtain

$$\vartheta(h) = \frac{180}{\pi R_e} \int_{h_0}^{h} \frac{V_E(z)}{V_z(z)}\, \mathrm{d}z \tag{3}$$

provided that the rate of climb of the stratospheric balloon $V_z \triangleq \mathrm{d}z/\mathrm{d}t \neq 0$. Now let us define the longitudinal trajectory prediction error (a similar expression can be obtained for the latitudinal error considering the north velocity component):

$$e_\vartheta(h) \stackrel{\text{def}}{=} \vartheta(h) - \vartheta_{\text{fc}}(h) = \frac{180}{\pi R_e} \int_{h_0}^{h} \frac{V_E}{V_z}\, \mathrm{d}z - \frac{180}{\pi R_e} \int_{h_0}^{h} \frac{V_{E_{\text{fc}}}}{V_{z_{\text{fc}}}}\, \mathrm{d}z \tag{4}$$

The subscript fc indicates those quantities that are obtained using the forecast data and related simulation:

$$e_\vartheta(h) \cong \frac{180}{\pi R_e} \int_{h_0}^{h} \left[\frac{\Delta V_E}{V_{z_{\text{fc}}}} + \left(-\frac{V_{E_{\text{fc}}}}{V_{z_{\text{fc}}}^2} \Delta V_z \right) \right] \mathrm{d}z \tag{5}$$

where Eq. (5) has been obtained using the following first-order Taylor expansion:

$$\begin{aligned} \frac{V_E}{V_z} &\cong \frac{V_{E_{\text{fc}}}}{V_{z_{\text{fc}}}} + \frac{\partial (V_E/V_z)}{\partial V_E} (V_E - V_{E_{\text{fc}}}) + \frac{\partial (V_E/V_z)}{\partial V_z} (V_z - V_{z_{\text{fc}}}) \\ &= \frac{V_{E_{\text{fc}}}}{V_{z_{\text{fc}}}} + \frac{\partial (V_E/V_z)}{\partial V_E} \Delta V_E + \frac{\partial (V_E/V_z)}{\partial V_z} \Delta V_z \end{aligned} \tag{6}$$

The balloon vertical velocity V_z is a function of the air pressure, air temperature, gas mass, and also other variables for which the related uncertainties will be assumed to be negligible (see Sec. II):

$$V_z^{\text{fc}} = f(p_{\text{air}}^{\text{fc}}, T_{\text{air}}^{\text{fc}}, M_{\text{gas}}^{\text{nom}}, \Pi_{\text{nom}}) \tag{7}$$

Using the first-order Taylor expansion of the actual vertical velocity V_z around the predicted vertical velocity V_z^{fc},

$$\begin{aligned} \Delta V_z = (V_z - V_z^{\text{fc}}) &\cong \frac{\partial f}{\partial p_{\text{air}}} (p_{\text{air}} - p_{\text{air}}^{\text{fc}}) + \frac{\partial f}{\partial T_{\text{air}}} (T_{\text{air}} - T_{\text{air}}^{\text{fc}}) \\ &+ \frac{\partial f}{\partial M_{\text{gas}}} (M_{\text{gas}} - M_{\text{gas}}^{\text{nom}}) = \frac{\partial f}{\partial p_{\text{air}}} \Delta p_{\text{air}} + \frac{\partial f}{\partial T_{\text{air}}} \Delta T_{\text{air}} \\ &+ \frac{\partial f}{\partial M_{\text{gas}}} \Delta M_{\text{gas}} \end{aligned} \tag{8}$$

Combining Eq. (5) with Eq. (8), we obtain

$$\begin{aligned} e_\vartheta(h) = \frac{180}{\pi R_e} \int_{h_0}^{h} \Bigg(&\frac{\Delta V_E}{V_{z_{\text{fc}}}} - \frac{V_{E_{\text{fc}}}}{V_{z_{\text{fc}}}^2} \frac{\partial f}{\partial p_{\text{air}}} \Delta p_{\text{air}} - \frac{V_{E_{\text{fc}}}}{V_{z_{\text{fc}}}^2} \frac{\partial f}{\partial T_{\text{air}}} \Delta T_{\text{air}} \\ &- \frac{V_{E_{\text{fc}}}}{V_{z_{\text{fc}}}^2} \frac{\partial f}{\partial M_{\text{gas}}} \Delta M_{\text{gas}} \Bigg) \mathrm{d}z \end{aligned} \tag{9}$$

Starting from Eq. (9), it is possible to compute the standard deviation of the ascent trajectory position error, assuming that the errors due to wind forecast, air temperature, air pressure, and gas mass are independent and zero mean (see the Appendix for mathematical details):

$$\begin{aligned} \sigma_{e_\vartheta}^2(h) = &\int_{h_0}^{h} \int_{h_0}^{h} \left[\frac{1}{V_{z_{\text{fc}}}(z_1)} \right] \left[\frac{1}{V_{z_{\text{fc}}}(z_2)} \right] R_{\Delta V_E}(z_1, z_2)\, \mathrm{d}z_1\, \mathrm{d}z_2 \\ &+ \int_{h_0}^{h} \int_{h_0}^{h} \left[\frac{V_{E_{\text{fc}}}(z_1)}{V_{z_{\text{fc}}}^2(z_1)} \frac{\partial f}{\partial p_{\text{air}}}(z_1) \right] \left[\frac{V_{E_{\text{fc}}}(z_2)}{V_{z_{\text{fc}}}^2(z_2)} \frac{\partial f}{\partial p_{\text{air}}}(z_2) \right] \\ &\times R_{\Delta p_{\text{air}}}(z_1, z_2)\, \mathrm{d}z_1\, \mathrm{d}z_2 + \int_{h_0}^{h} \int_{h_0}^{h} \left[\frac{V_{E_{\text{fc}}}(z_1)}{V_{z_{\text{fc}}}^2(z_1)} \frac{\partial f}{\partial T_{\text{air}}}(z_1) \right] \\ &\times \left[\frac{V_{E_{\text{fc}}}(z_2)}{V_{z_{\text{fc}}}^2(z_2)} \frac{\partial f}{\partial T_{\text{air}}}(z_2) \right] R_{\Delta T_{\text{air}}}(z_1, z_2)\, \mathrm{d}z_1\, \mathrm{d}z_2 \\ &+ \int_{h_0}^{h} \int_{h_0}^{h} \left[\frac{V_{E_{\text{fc}}}(z_1)}{V_{z_{\text{fc}}}^2(z_1)} \frac{\partial f}{\partial M_{\text{gas}}}(z_1) \right] \left[\frac{V_{E_{\text{fc}}}(z_2)}{V_{z_{\text{fc}}}^2(z_2)} \frac{\partial f}{\partial M_{\text{gas}}}(z_2) \right] \\ &\times R_{\Delta M_{\text{gas}}}(z_1, z_2)\, \mathrm{d}z_1\, \mathrm{d}z_2 \end{aligned} \tag{10}$$

where $R_x(z_1, z_2) \triangleq E\{x(z_1)x(z_2)\}$ is the autocorrelation function of the generic stochastic process $x(z)$.

Therefore, it is sufficient to compute the autocorrelation function of the ECMWF forecast errors (wind, air temperature, and air pressure) and of the gas mass error and to numerically solve the integral of the Eq. (10) to obtain the statistical characterization of the position error $e_\vartheta(h)$.

ECMWF forecast uncertainty characterization in terms of wind, air temperature, and pressure has been carried out performing a statistical analysis based on a set of ECMWF forecast and analysis data relative to Arbatax (DTFT1 mission launch base) during the years 2004–2008. Forecast data provide the predicted wind (north and east components) and the predicted air pressure and temperature as a function of the altitude, latitude, and longitude. These data have been compared to the analysis data (which are assumed to be the *true* atmospheric and wind data) in order to perform a statistical characterization of the ECMWF prediction error at −6, −18, −30, −42, −54, and −66 h before a given reference time (launch time). In this characterization, the prediction errors do not depend on latitude and longitude. This last assumption can be justified considering that above a certain altitude the atmospheric and wind prediction errors are mainly due to inaccuracies in the IFS model and not to possible orographic effects over the geographical region considered. Indeed, in the lowermost troposphere, the spatial resolution of the ECMWF model may poorly represent the local orography and may therefore introduce local prediction errors that cannot be taken into account, whereas at higher altitudes, the orographic effects become gradually less influential.

Finally, we have characterized the errors due to the inflation procedures (ΔM_{gas}) as a zero-mean Gaussian random variable, with a maximum error ($3\sigma_{\Delta M}$) of 2% with respect to the nominal mass of gas $M_{\text{gas}}^{\text{nom}}$. This implies that the autocorrelation function is constant for each altitude, i.e. $R_{\Delta M_{\text{gas}}}(z_1, z_2) = \sigma_{\Delta M}^2$.

Concerning the terms $\partial f/\partial p_{\text{air}}$, $\partial f/\partial T_{\text{air}}$, and $\partial f/\partial M_{\text{gas}}$ in Eq. (10), they have been obtained starting from the vertical equation of motion of a balloon under zero vertical acceleration [6] and considering that for zero-pressure balloons the assumption $p_{\text{gas}} \cong p_{\text{air}}$ holds:

$$V_z^2 \cong -\frac{2M_{\text{gross}}g}{\rho_{\text{air}}C_D A_{\text{drag}}}\left[1+\frac{M_{\text{gas}}}{M_{\text{gross}}}\left(1-\frac{\rho_{\text{air}}}{\rho_{\text{gas}}}\right)\right] = -\frac{2M_{\text{gross}}gR_{\text{air}}}{T_{\text{gas}}^{\frac{2}{3}}R_{\text{gas}}^{\frac{2}{3}}C_D k}T_{\text{air}}p_{\text{air}}^{-\frac{1}{3}}M_{\text{gas}}^{-\frac{2}{3}}\left[1+\frac{M_{\text{gas}}}{M_{\text{gross}}}\left(1-\frac{T_{\text{gas}}\sigma}{T_{\text{air}}}\right)\right] \quad (11)$$

where $A_{\text{drag}} = k \cdot \text{vol}^{\frac{2}{3}}$, k is a geometric factor, and σ is the ratio between the molecular weight of air and the molecular weight of the gas. In effect, Eq. (11) gives a good approximation of the vertical velocity during the whole balloon ascent, except for those phases in which the acceleration cannot be considered zero (liftoff, tropopause transition, stratospheric oscillations, or local wind shears).

It is now possible to calculate the partial derivatives assuming that T_{gas} is independent of T_{air}, p_{air}, and M_{gas}:

$$\frac{\partial V_z}{\partial T_{\text{air}}} = -\frac{1}{2V_z}\cdot\frac{2M_{\text{gross}}gR_{\text{air}}}{T_{\text{gas}}^{\frac{2}{3}}R_{\text{gas}}^{\frac{2}{3}}C_D k}p_{\text{air}}^{-\frac{1}{3}}M_{\text{gas}}^{-\frac{2}{3}}\left(1+\frac{M_{\text{gas}}}{M_{\text{gross}}}\right) \quad (12)$$

$$\frac{\partial V_z}{\partial p_{\text{air}}} = \frac{1}{2V_z}\cdot\frac{2M_{\text{gross}}gR_{\text{air}}}{3T_{\text{gas}}^{\frac{2}{3}}R_{\text{gas}}^{\frac{2}{3}}C_D k}T_{\text{air}}p_{\text{air}}^{-\frac{4}{3}}M_{\text{gas}}^{-\frac{2}{3}}\left[1+\frac{M_{\text{gas}}}{M_{\text{gross}}}\left(1-\frac{T_{\text{gas}}\sigma}{T_{\text{air}}}\right)\right] \quad (13)$$

$$\frac{\partial V_z}{\partial M_{\text{gas}}} = \frac{1}{2V_z}\cdot\left\{-\frac{2M_{\text{gross}}gR_{\text{air}}}{T_{\text{gas}}^{\frac{2}{3}}R_{\text{gas}}^{\frac{2}{3}}C_D k}T_{\text{air}}p_{\text{air}}^{-\frac{1}{3}}\left[-\frac{2}{3}M_{\text{gas}}^{-\frac{5}{3}} + \frac{M_{\text{gas}}^{-\frac{2}{3}}}{3M_{\text{gross}}}\left(1-\frac{T_{\text{gas}}\sigma}{T_{\text{air}}}\right)\right]\right\} \quad (14)$$

To validate the results that can be obtained using these derivatives, a numerical analysis was carried out. In particular, the analytical derivatives computed by means of Eqs. (12–14) have been compared to the numerical derivatives obtained computing (using ACHAB) the variation of the vertical velocity due to perturbed profiles of T_{air} and p_{air}, as well as perturbed values of M_{gas}.

The results of this comparative analysis were generally satisfactory. However, Eq. (14) guarantees a good agreement only up to the tropopause, thus suggesting that the approximation by which T_{gas} is independent of M_{gas} is not valid throughout the whole ascent trajectory. Therefore, in order to get a more accurate expression of the partial derivative $\partial V_z/\partial M_{\text{gas}}$, it is necessary to consider explicitly the dependence of T_{gas} on M_{gas}. In general, this is not an easy task because these quantities are related to each other through a thermodynamic differential equation:

$$\dot{T}_{\text{gas}} = \frac{Q_{\text{IntConv}}}{\gamma c_v M_{\text{gas}}} - \frac{(\gamma-1)}{\gamma}\frac{\rho_{\text{air}}g}{\rho_{\text{gas}}R_{\text{gas}}}\cdot V_z \quad (15)$$

In view of this consideration, we tried to solve this problem by making the following hypotheses:

1) The derivative of the gas temperature after the tropopause is negligible: $\dot{T}_{\text{gas}} \cong 0$. In fact, before the tropopause, the contribution of the convective heat load Q_{IntConv} in Eq. (15) is negligible compared to the adiabatic contribution. After the tropopause, the two terms become comparable, at least during the ascent phase, causing $\dot{T}_{\text{gas}}$ to become negligible with respect to its value in the troposphere.

2) The internal convective heat load is dependent on the gas mass only through the gas temperature. In fact, even if the internal convective heat load $Q_{\text{IntConv}} = h_{\text{conv}}A_{\text{eff}}(T_{\text{film}} - T_{\text{gas}})$ depends on M_{gas} not only through T_{gas} but also through h_{conv}, A_{eff}, and T_{film}, we have decided to neglect these last dependencies for our scopes, considering that the gas temperature is the most sensitive variable to gas mass variations.

With the above hypotheses, we can write the gas temperature as

$$T_{\text{gas}} \cong \frac{Q_{\text{IntConv}}}{c_v M_{\text{gas}}}\frac{T_{\text{air}}R_{\text{air}}}{g(\gamma-1)V_z} \Rightarrow T_{\text{gas}} \cong \frac{HT_{\text{film}}K'}{M_{\text{gas}}V_z + HK'} \quad (16)$$

where $H = h_{\text{conv}}A_{\text{eff}}$, and

$$K' = \frac{T_{\text{air}}R_{\text{air}}}{c_v g(\gamma-1)}$$

Combining Eq. (11) with Eq. (16), we obtain a new (implicit) equation for V_z:

$$V_z^2 \cong \frac{A}{M_{\text{gas}}^{\frac{2}{3}}}[B(V_z M_{\text{gas}} + HK')]^{\frac{2}{3}} + \frac{AM_{\text{gas}}^{\frac{1}{3}}}{M_{\text{gross}}}[B(V_z M_{\text{gas}} + HK')]^{\frac{2}{3}} + -\frac{AM_{\text{gas}}^{\frac{1}{3}}}{M_{\text{gross}}}\rho_{\text{air}}[B(V_z M_{\text{gas}} + HK')]^{-\frac{1}{3}} = G(V_z, M_{\text{gas}}, \Omega) \quad (17)$$

where

$$A = -\frac{2M_{\text{gross}}g}{\rho_{\text{air}}C_D k}$$

$$B = \frac{p_{\text{air}}}{R_{\text{gas}}HT_{\text{film}}K'}$$

and Ω are the variables that are assumed to be independent of V_z and M_{gas}.

The derivative $\partial V_z/\partial M_{\text{gas}}$ after the tropopause can be computed by taking the derivative of both the right and left sides of Eq. (17) with respect to the gas mass, applying the chain rule:

$$\frac{\partial(V_z^2)}{\partial V_z}\frac{\partial V_z}{\partial M_{\text{gas}}} = \frac{\partial G}{\partial M_{\text{gas}}} + \frac{\partial G}{\partial V_z}\frac{\partial V_z}{\partial M_{\text{gas}}} \Rightarrow \frac{\partial V_z}{\partial M_{\text{gas}}} = \left(1-\left(\frac{\partial G}{\partial V_z}\Big/\frac{\partial(V_z^2)}{\partial V_z}\right)\right)^{-1}\left(\frac{\partial G}{\partial M_{\text{gas}}}\Big/\frac{\partial(V_z^2)}{\partial V_z}\right) \quad (18)$$

Note that Eq. (18) is well defined since it can be easily shown that

$$\left(1-\frac{\partial G}{\partial V_z}\Big/\frac{\partial(V_z^2)}{\partial V_z}\right)$$

is strictly greater than zero.

Finally, the comparative numerical analysis has shown that the $\partial V_z/\partial M_{\text{gas}}$ computed by Eq. (14) before the tropopause and by

Eq. (18) after the tropopause guarantees a satisfactory agreement between the analytical and numeric derivative.

In the next section, the effectiveness and reliability of this approach will be demonstrated by means of a Monte Carlo analysis, which accounts for atmospheric and wind dispersions and gas inflation errors.

IV. Results

To demonstrate the effectiveness of the proposed approach, a Monte Carlo analysis can be carried out starting from a predicted trajectory and adding atmospheric, wind, and inflation errors according to their statistical characterization. As an example, we report the results of the Monte Carlo analysis performed considering the atmospheric and wind forecast data at −18 h before the launch and their related uncertainties as well as the inflation errors. We have obtained a set of trajectories dispersed around the predicted trajectory that has been used to verify the reliability of the estimation of the ascent trajectory prediction error.

The methodology presented in Sec. III allows computing the standard deviations (as a function of the altitude) of the ascent trajectory position errors for both the longitudinal and the latitudinal errors, $\sigma_{e_\vartheta}(h)$ and $\sigma_{e_\lambda}(h)$. These two standard deviations can be used to draw an ellipse for which the area contains the position of the actual trajectory with a given level of probability (longitudinal and latitudinal errors have been assumed as Gaussian and independent) [6]. The purpose of the Monte Carlo analysis is then to verify that the estimation of the standard deviations is sufficiently accurate; that is, the drawn ellipse actually includes the percentage of the dispersed trajectories corresponding to the given probability level.

The predicted trajectory has been computed using the ECMWF forecast data relative to 24 February 2007 at −18 h before the launch and a nominal gas mass $M_{\text{gas}}^{\text{nom}} = 792$ kg. The resulting trajectory is shown in Fig. 2.

The black circle in Fig. 2 represents the predicted position of the balloon at an altitude of 30 km. Concerning the prediction uncertainties (wind, air temperature, air pressure, and gas mass), we consider the following statistical characterization:

1) The wind forecast error is a Gaussian wide-sense stationary stochastic process with zero-mean and autocorrelation functions $R_{\Delta V_E}(z_1, z_2) = R_{\Delta V_E}(z_1 - z_2)$ and $R_{\Delta V_N}(z_1, z_2) = R_{\Delta V_N}(z_1 - z_2)$ for the east and north components, respectively. These autocorrelation functions have been numerically estimated and they are depicted in Fig. 3.

2) The temperature and pressure forecast errors are Gaussian wide-sense stationary stochastic processes with zero-mean and autocorrelation functions $R_{\Delta T_{\text{air}}}(z_1, z_2) = R_{\Delta T_{\text{air}}}(z_1 - z_2)$ and $R_{\Delta p_{\text{air}}}(z_1, z_2) = R_{\Delta p_{\text{air}}}(z_1 - z_2)$ respectively. These autocorrelation functions have been numerically estimated and they are depicted in Fig. 4.

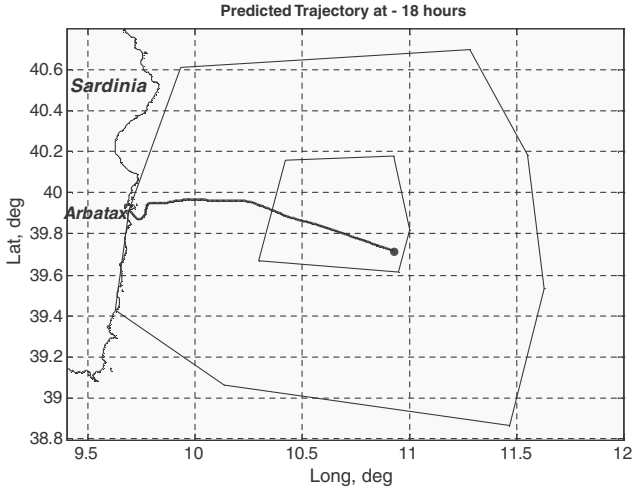

Fig. 2 Predicted trajectory at −18 h.

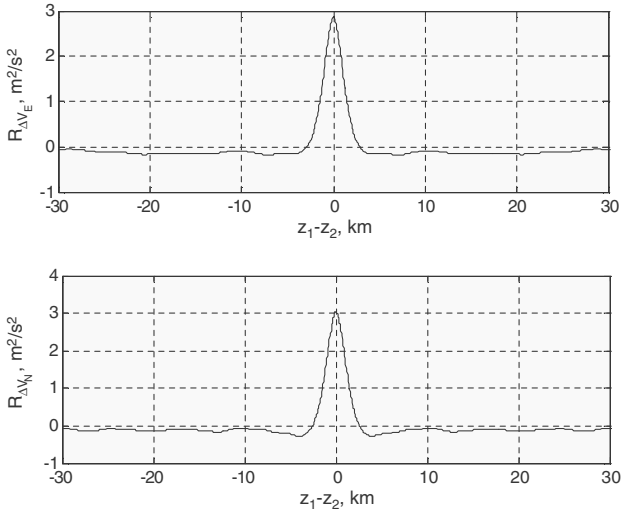

Fig. 3 Autocorrelation functions of the wind forecast errors (at −18 h).

3) The gas mass error is a zero-mean Gaussian random variable, with a standard deviation

$$\sigma_{\Delta M} = M_{\text{gas}}^{\text{nom}} \cdot 0.02/3 = 792 \text{ kg} \cdot 0.02/3 = 5.28 \text{ kg}$$

(see Sec. III).

To reproduce a Gaussian process with a given autocorrelation function, the following approach has been used: first, the autocorrelation functions of Fig. 3 and 4 have been approximated as autocorrelation functions having the following shape:

$$R_x(z_1 - z_2) = R_x^0 e^{-\frac{|z_1 - z_2|}{Z}}$$

where x is a generic stochastic process. Once the parameters R_x^0 and Z are estimated from the numerical data, the stochastic process x can be easily modeled by passing a Gaussian white noise w with variance $\sigma_w^2 = 2R_x^0/\tau$ through a first-order low-pass filter with transfer function $P(s) = \tau/(s\tau + 1)$, where $\tau = Z/|V_z|$.

Now it is possible to calculate [using Eq. (10)] the standard deviations of the ascent trajectory prediction errors $\sigma_{e_\vartheta}(h)$ and $\sigma_{e_\lambda}(h)$ for $h = 30$ km and to draw the elliptic dispersion area as explained above. Using the predicted trajectory computed with the ECMWF forecast data relative to 24 February 2007 at −18 h before the launch and a nominal gas mass $M_{\text{gas}}^{\text{nom}} = 792$ kg, we obtain the following standard deviations:

$$\sigma_{e_\vartheta}(h = 30 \text{ km}) = 5883 \text{ m} \qquad \sigma_{e_\lambda}(h = 30 \text{ km}) = 3915 \text{ m} \quad (19)$$

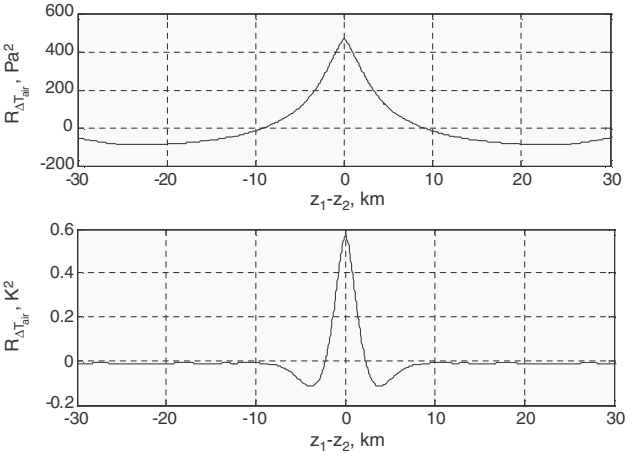

Fig. 4 Autocorrelation functions of the air pressure and air temperature forecast errors (at −18 h).

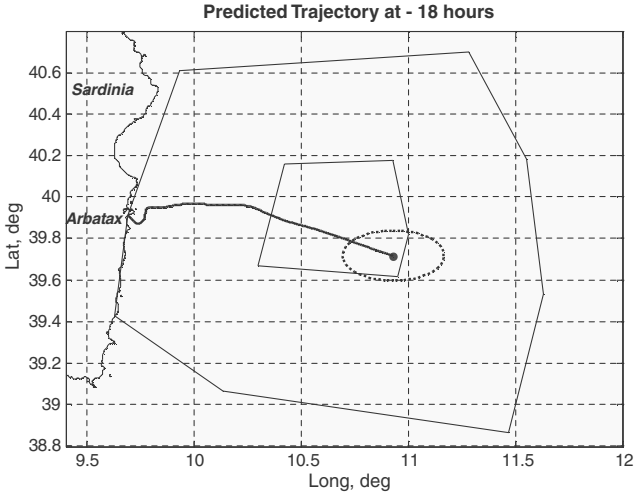

Fig. 5 Dispersion area (dotted ellipse).

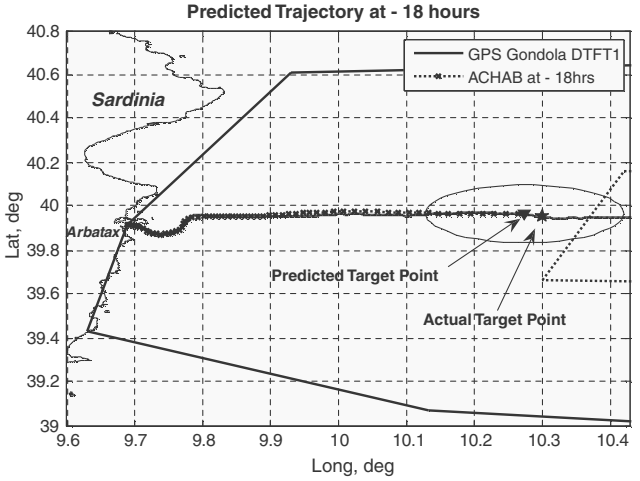

Fig. 8 Comparison between actual flight data and ACHAB's prediction with the related dispersion area.

For instance, these two standard deviations can be used to draw an ellipse for which the area contains the position of the actual trajectory with a probability of 99.7%. Figure 5 shows the predicted trajectory and the related estimation of the prediction error.

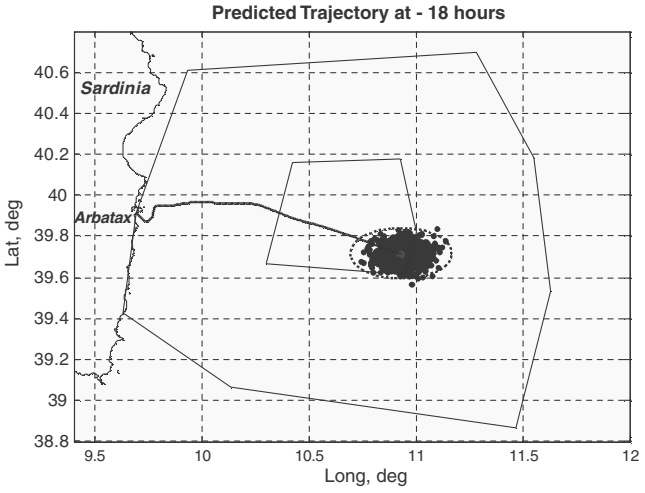

Fig. 6 Monte Carlo analysis: position of the dispersed trajectories at 30 km of altitude.

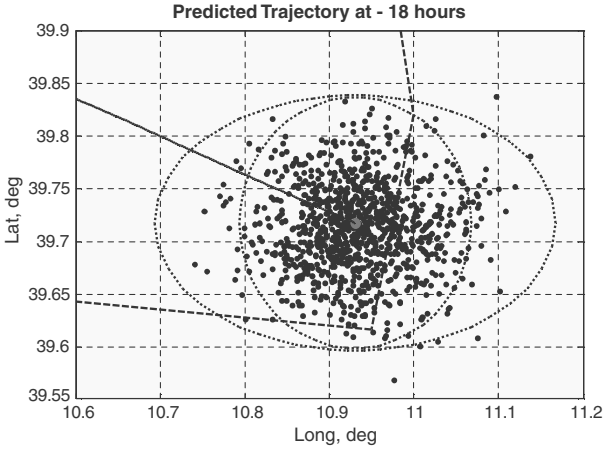

Fig. 7 Comparison between the dispersion area obtained using the proposed approach (outermost ellipse) and the one reported in [6] (innermost ellipse).

Starting from the described uncertainty characterization, 1000 trajectories have been simulated. Figure 6 reports the position of each trajectory at an altitude of 30 km. As it can be seen from Fig. 6, almost the totality of the dispersed points lie inside the ellipse. In particular, only six points fall outside the dispersion ellipse; therefore, the area contains $994/1000 = 99.4\%$ of the dispersed trajectories, thus confirming the effectiveness of the trajectory error estimation.

The comparison between the dispersion area obtained using the proposed approach and the one reported in [6] is depicted in Fig. 7 in order to show the improvement achieved in the accuracy of the estimation of the trajectory prediction error. In particular, it can be seen that only $947/1000 = 94.7\%$ of dispersed points lie inside the ellipse.

As an example of practical application, it is possible to compare the results of the proposed approach to the balloon ascent trajectory flown during the execution of the DTFT1 mission carried out on 24 February 2007 (see Fig. 8). As shown in Fig. 8, the position of the actual target point is well predicted.

V. Conclusions

In this paper, a methodology for the estimation of the trajectory prediction errors of a balloon ascent flight has been developed. In this approach, uncertainties on wind velocity forecast, on air temperature forecast, on air pressure forecast, and on the quantity of gas transferred to the balloon due to inflation procedures are taken into account and propagated on the balloon's velocity vector. Using an approach based on the theory of error propagation, this methodology allows effectively estimating the dispersion of the actual trajectory via an analytic relationship once the predicted ascent trajectory is computed using forecast data.

The proposed approach is able to evaluate the uncertainty related to a given predicted ascent trajectory in a simple and reliable manner. Specifically, it allows statistically estimating the position error for each altitude, thus obtaining dispersion areas that contain the actual trajectory with a given level of probability.

Validation of the methodology has been carried out via a Monte Carlo analysis that confirmed the effectiveness of the trajectory error estimation, demonstrating the improvement obtained when also taking into account the uncertainties on the vertical velocity component of the stratospheric balloon.

Appendix: Standard Deviation of the Position Error

In this Appendix, further details on the derivation of Eq. (10) are given. Starting from Eq. (9), it is possible to compute the standard deviation of the ascent trajectory position error, assuming that the errors due to wind forecast, air temperature, air pressure, and gas mass are independent and zero mean:

$$\sigma^2_{e_\vartheta}(h) = E\{e^2_\vartheta(h)\} = E\left\{\left(\int_{h_0}^{h} \frac{1}{V_{z_{\rm fc}}}\Delta V_E\,{\rm d}z\right)^2\right\} + E\left\{\left(\int_{h_0}^{h} -\frac{V_{E_{\rm fc}}}{V^2_{z_{\rm fc}}}\frac{\partial f}{\partial p_{\rm air}}\Delta p_{\rm air}\,{\rm d}z\right)^2\right\} + E\left\{\left(\int_{h_0}^{h} -\frac{V_{E_{\rm fc}}}{V^2_{z_{\rm fc}}}\frac{\partial f}{\partial T_{\rm air}}\Delta T_{\rm air}\,{\rm d}z\right)^2\right\} + E\left\{\left(\int_{h_0}^{h} -\frac{V_{E_{\rm fc}}}{V^2_{z_{\rm fc}}}\frac{\partial f}{\partial M_{\rm gas}}\Delta M_{\rm gas}\,{\rm d}z\right)^2\right\} \tag{A1}$$

where $E\{\cdot\}$ is the statistical mean operator. Equation (A1) can be rewritten as

$$\sigma^2_{e_\vartheta}(h) = E\left\{\int_{h_0}^{h} \frac{1}{V_{z_{\rm fc}}}\Delta V_E\,{\rm d}z_1 \int_{h_0}^{h} \frac{1}{V_{z_{\rm fc}}}\Delta V_E\,{\rm d}z_2\right\} + E\left\{\int_{h_0}^{h} \frac{V_{E_{\rm fc}}}{V^2_{z_{\rm fc}}}\frac{\partial f}{\partial p_{\rm air}}\Delta p_{\rm air}\,{\rm d}z_1 \int_{h_0}^{h} \frac{V_{E_{\rm fc}}}{V^2_{z_{\rm fc}}}\frac{\partial f}{\partial p_{\rm air}}\Delta p_{\rm air}\,{\rm d}z_2\right\} + E\left\{\int_{h_0}^{h} \frac{V_{E_{\rm fc}}}{V^2_{z_{\rm fc}}}\frac{\partial f}{\partial T_{\rm air}}\Delta T_{\rm air}\,{\rm d}z_1 \int_{h_0}^{h} \frac{V_{E_{\rm fc}}}{V^2_{z_{\rm fc}}}\frac{\partial f}{\partial p_{\rm air}}\Delta T_{\rm air}\,{\rm d}z_2\right\} + E\left\{\int_{h_0}^{h} \frac{V_{E_{\rm fc}}}{V^2_{z_{\rm fc}}}\frac{\partial f}{\partial M_{\rm gas}}\Delta M_{\rm gas}\,{\rm d}z_1 \int_{h_0}^{h} \frac{V_{E_{\rm fc}}}{V^2_{z_{\rm fc}}}\frac{\partial f}{\partial M_{\rm gas}}\Delta M_{\rm gas}\,{\rm d}z_2\right\} \tag{A2}$$

Considering that the statistical mean is a linear operator, it can be interchanged with the integral operator, thus obtaining

$$\sigma^2_{e_\vartheta}(h) = \int_{h_0}^{h}\int_{h_0}^{h}\left[\frac{1}{V_{z_{\rm fc}}(z_1)}\right]\left[\frac{1}{V_{z_{\rm fc}}(z_2)}\right]E\{\Delta V_E(z_1)\Delta V_E(z_2)\}\,{\rm d}z_1\,{\rm d}z_2 + \int_{h_0}^{h}\int_{h_0}^{h}\left[\frac{V_{E_{\rm fc}}(z_1)}{V^2_{z_{\rm fc}}(z_1)}\frac{\partial f}{\partial p_{\rm air}}(z_1)\right]\left[\frac{V_{E_{\rm fc}}(z_2)}{V^2_{z_{\rm fc}}(z_2)}\frac{\partial f}{\partial p_{\rm air}}(z_2)\right] \times E\{\Delta p_{\rm air}(z_1)\Delta p_{\rm air}(z_2)\}\,{\rm d}z_1\,{\rm d}z_2 + \int_{h_0}^{h}\int_{h_0}^{h}\left[\frac{V_{E_{\rm fc}}(z_1)}{V^2_{z_{\rm fc}}(z_1)}\frac{\partial f}{\partial T_{\rm air}}(z_1)\right] \times \left[\frac{V_{E_{\rm fc}}(z_2)}{V^2_{z_{\rm fc}}(z_2)}\frac{\partial f}{\partial T_{\rm air}}(z_2)\right]E\{\Delta T_{\rm air}(z_1)\Delta T_{\rm air}(z_2)\}\,{\rm d}z_1\,{\rm d}z_2 + \int_{h_0}^{h}\int_{h_0}^{h}\left[\frac{V_{E_{\rm fc}}(z_1)}{V^2_{z_{\rm fc}}(z_1)}\frac{\partial f}{\partial M_{\rm gas}}(z_1)\right]\left[\frac{V_{E_{\rm fc}}(z_2)}{V^2_{z_{\rm fc}}(z_2)}\frac{\partial f}{\partial M_{\rm gas}}(z_2)\right] \times E\{\Delta M_{\rm gas}(z_1)\Delta M_{\rm gas}(z_2)\}\,{\rm d}z_1\,{\rm d}z_2 \tag{A3}$$

Introducing the autocorrelation function of the generic stochastic process $x(z)$, $R_x(z_1, z_2) \triangleq E\{x(z_1)x(z_2)\}$, we finally obtain

$$\sigma^2_{e_\vartheta}(h) = \int_{h_0}^{h}\int_{h_0}^{h}\left[\frac{1}{V_{z_{\rm fc}}(z_1)}\right]\left[\frac{1}{V_{z_{\rm fc}}(z_2)}\right]R_{\Delta V_E}(z_1, z_2)\,{\rm d}z_1\,{\rm d}z_2 + \int_{h_0}^{h}\int_{h_0}^{h}\left[\frac{V_{E_{\rm fc}}(z_1)}{V^2_{z_{\rm fc}}(z_1)}\frac{\partial f}{\partial p_{\rm air}}(z_1)\right]\left[\frac{V_{E_{\rm fc}}(z_2)}{V^2_{z_{\rm fc}}(z_2)}\frac{\partial f}{\partial p_{\rm air}}(z_2)\right] \times R_{\Delta p_{\rm air}}(z_1, z_2)\,{\rm d}z_1\,{\rm d}z_2 + \int_{h_0}^{h}\int_{h_0}^{h}\left[\frac{V_{E_{\rm fc}}(z_1)}{V^2_{z_{\rm fc}}(z_1)}\frac{\partial f}{\partial T_{\rm air}}(z_1)\right] \times \left[\frac{V_{E_{\rm fc}}(z_2)}{V^2_{z_{\rm fc}}(z_2)}\frac{\partial f}{\partial T_{\rm air}}(z_2)\right]R_{\Delta T_{\rm air}}(z_1, z_2)\,{\rm d}z_1\,{\rm d}z_2 + \int_{h_0}^{h}\int_{h_0}^{h}\left[\frac{V_{E_{\rm fc}}(z_1)}{V^2_{z_{\rm fc}}(z_1)}\frac{\partial f}{\partial M_{\rm gas}}(z_1)\right]\left[\frac{V_{E_{\rm fc}}(z_2)}{V^2_{z_{\rm fc}}(z_2)}\frac{\partial f}{\partial M_{\rm gas}}(z_2)\right] \times R_{\Delta M_{\rm gas}}(z_1, z_2)\,{\rm d}z_1\,{\rm d}z_2 \tag{A4}$$

References

[1] Palumbo, R., Mercogliano, P., Corraro, F., De Matteis, P. P., and Sabatano, R., "Meteorological Conditions Forecast and Balloon Trajectory Estimations," *Memorie Della Società Astronomica Italiana*, Vol. 79, No. 3, 2008, pp. 841–845.

[2] Russo, G., Carmicino, C., de Matteis, P., Marini, M., Rufolo, G., Di Palma, L., et al., "Unmanned Space Vehicle Program: DTFT in Flight Experiments," *18th ESA Symposium on European Rocket and Balloon Programmes and Related Research*, ESA Communication Production Office, European Space Research and Technology Center, Noordwijk, The Netherlands, Nov. 2007, pp. 89–96. Visby, Sweden, 2007.

[3] Musso, I., Cardillo, A., Cosentino, O., and Memmo, A., "A Balloon Trajectory Prediction System," *Advances in Space Research*, Vol. 33, No. 10, 2004, pp. 1722–1726. doi:10.1016/j.asr.2003.07.044

[4] Musso, I., Cardillo, A., Ibba, R., Spoto, D., Peterzen, S., Masi, S., and Memmo, A., "Enhancement on Stratospheric Balloons Trajectory Prediction, Optimization and Monitoring," *18th ESA Symposium on European Rocket and Balloon Programmes and Related Research*, European Space Research and Technology Center, Noordwijk, The Netherlands, Nov. 2007, pp. 331–336.

[5] Collander, R. S., and Girz, C. M. I. R., "Evaluation of Balloon Trajectory Forecast Routines for Gains," *Advances in Space Research*, Vol. 33, No. 10, The Next Generation in Scientific Ballooning, 2004, pp. 1727–1731. doi:10.1016/j.asr.2003.05.016

[6] Morani, G., Palumbo, R., Cuciniello, G., Corraro, F., and Russo, M., "Method for Prediction and Optimization of a Stratospheric Balloon Ascent Trajectory," *Journal of Spacecraft and Rockets*, Vol. 46, No. 1, Jan.–Feb. 2009, pp. 126–133. doi:10.2514/1.39469

[7] Palumbo, R., Russo, M., Filippone, E., and Corraro, F., "ACHAB: Analysis Code for High-Altitude Balloons," AIAA Atmospheric Flight Mechanics Conference and Exhibit, Hilton Head Island, SC, AIAA Paper 2007-6642, 2007.

[8] Morris, A. (Ed.), "Scientific Ballooning Handbook," National Center for Atmospheric Research TN/1A-99, Boulder, CO, 1975.

[9] Conrad, G. R., and Robbins, E. J., "Determination of Balloon Drag," AIAA International Balloon Technology Conference, AIAA Paper 1991-3666, Albuquerque, NM, Oct. 1991.